Vestigial like 4 regulates the adipogenesis of classical brown adipose tissue

Running title: VGLL4 regulates brown adipose tissue development

Pingzhu Zhou[a, *, &], Chase W. Kessinger[b, *], Fei Gu[a], Amanda Davenport[b], Justin S. King[a], Genyu Wang[b], Steven G. Negron[b], Bart Deplancke[c], William T. Pu[a], Zhiqiang Lin[b, #].

a. Boston Children's Hospital, 300 Longwood Ave, Boston, MA, 02115

b. Department of Biomedical Research and Translational Medicine, Masonic Medical Research Institute, 2150 Bleecker St, Utica, NY 13501

c. Swiss Institute of Bioinformatics, CH-1015 Lausanne, Switzerland

&. Current affiliation: Shanghai 411 Hospital, School of Medicine, Shanghai University, 99 Shangda Road, Shanghai, 200444, China.

*P. Z. and C.W.K contributed equally to this work.

[#] To whom correspondence should be addressed: zlin@mmri.edu

Abstract

Brown adipose tissue (BAT) is mammals' primary non-shivering thermogenesis organ, and the molecular mechanisms regulating BAT growth and adipogenesis are largely unknown. The Hippo-YAP pathway has been well-known for controlling organ size, and Vestigial like 4 (VGLL4) is a transcriptional regulator that modulates the Hippo-YAP pathway by competing against YAP for binding to TEAD proteins. In this study, we dissected the function of VGLL4 in regulating BAT development. We generated a conventional *Vgll4* mutant mouse line, in which the two Tondu (TDU) domains of VGLL4 were disrupted. We found that deletion of the TDU domains of VGLL4 resulted in perinatal lethality and paucity of the interscapular BAT. Histological and magnetic resonance imaging studies confirmed that the adipogenesis of BAT was impaired in *Vgll4* mutants. Adeno-associated virus (AAV) mediated, brown adipocyte-specific overexpression of VGLL4 increased BAT volume and protected the adult male mice from acute cold stress. Genomic studies suggest that VGLL4/TEAD1 complex directly regulates the myogenic and adipogenic gene expression programs of BAT. In conclusion, our data identify VGLL4 as a previously unrecognized adipogenesis factor that regulates classical BAT development.

Keywords: Vestigial like 4, TEAD1, CEBPβ, Hippo-YAP pathway, classical brown adipose tissue, development, adipogenesis.

Introduction

Obesity is a global epidemic that contributes to a number of chronic disease conditions, such as type 2 diabetes mellitus, non-alcoholic fatty liver, cardiovascular disease, and cancers [1]. In mammals, the adipose tissue comprises white and brown adipose tissue (WAT and BAT, respectively) [2]. WAT stores triglycerides in adipocytes, and its expansion is a hallmark of obesity. On the other hand, BAT burns triglycerides and glucose to generate heat [3]. Based on its developmental origin, BAT is further divided into classical BAT and white adipocyte-derived brown adipocytes (beige/brite cells) [4]. In humans, BAT is abundant in infants, and decreases with age [5]. Recently, the discovery of functional BAT and beige cells in adults [6] raises the possibility of treating obesity by activating BAT or increasing the browning of WAT [7]**.** Thus understanding the molecular mechanisms that control BAT growth and function is critical for developing therapeutic strategies to treat obesity.

Both white adipocytes and classical brown adipocytes (BACs) are derived from mesenchymal stem cells [8]. BAC adipogenesis generally includes four steps. First, mesenchymal stem cells differentiate into myogenic factor 5 (Myf5)-expressing progenitor cells. Next, Myf5^{+} progenitor cells differentiate into brown preadipocytes, which then differentiate into UCP1-positive naive BACs. Finally, naive BACs develop into lipid-loaded and mitochondria abundant mature BACs [9]. In mice, the interscapular BAT depot appears at embryonic day 15.5 (E15.5), and expands rapidly during fetal and neonatal development. BAT lipogenesis is minimal in murine embryos and increases remarkably after birth [10,11].

The genetic programs controlling BAT adipogenesis are well documented. Transcription factors, including peroxisome proliferator-activated receptor gamma (PPARγ), CCAAT/ enhancer-binding proteins (specifically CEBPβ/δ), and PRD1-BF-1-RIZ1 homologous domain containing protein-16 (PRDM16), are key regulators of BAC differentiation [8,9,12]. Conditional deletion of *Pparg* in adipocytes reduced both WAT and BAT [13]. Mice missing both CEBPβ and CEBPδ had no lipid accumulation in BAT, and primary embryonic fibroblasts lacking both of these factors failed to undergo adipocyte differentiation [14]. PRDM16 is a crucial regulator of myogenic and brown adipogenic lineage differentiation, because ectopic expression of PRDM16 in myoblasts activated the BAC differentiation program, which relied on the interaction between PRDM16 and CEBPβ/δ [15].

The Hippo-YAP kinase signaling pathway is well known for controlling organ growth [16]. In mammals, upstream signaling pathways activate the Hippo kinase cascade, comprised of MST1/2, LATS1/2, and the scaffold protein Salvador (Sav). Activation of this kinase cascade

64 results in phosphorylation and inactivation of YAP and WWTR1 (more commonly referred to
65 as TAZ), orthologous transcriptional co-activators that are terminal transcriptional effectors of
66 this pathway. YAP/TAZ interact with TEAD family transcription factors to regulate downstream
67 target gene expression, including genes that control cell proliferation [17]. Several studies have
68 implicated Hippo-YAP signaling in WAT adipogenesis. In the 3T3-L1 preadipocyte cell line,
69 which has been widely used to study WAT adipocyte differentiation [18], overexpression or
70 knock-down of Hippo kinases activated or suppressed adipogenesis, respectively [19,20], while
71 knock-down of YAP/TAZ or TEAD4 augmented WAT adipogenesis [21,22]. YAP/TAZ-TEAD
72 complex also plays an important role in regulating BAT adipogenesis. BAT-specific YAP/TAZ
73 double heterozygous mice (YTU) had reduced BAT size and impaired metabolic activity at 4
74 weeks of age. At 20 weeks of age, compared with the BAT of the age matched control mice,
75 the YTU BAT was two times larger, which was due to excessive lipid accumulation in the
76 BACs [23]. However, the underlying molecular mechanism of how YAP/TAZ-TEAD complex
77 regulates BAT adipogenesis has not been well documented.
78 In addition to inhibition by the Hippo kinase cascade, the activity of the YAP/TAZ-TEAD
79 complex is also suppressed by Vestigial like 4 (VGLL4), a transcriptional regulator that
80 competes with YAP/TAZ for binding to TEAD [24,25]. In 3T3-L1 cells, loss of either TEAD4 or
81 VGLL4 increased adipogenesis; overexpressing TEAD4 suppressed adipogenesis, which was
82 abolished by knocking down VGLL4 [22]. These data highlight the importance of VGLL4 as a
83 crucial regulator of adipogenesis in vitro and raise the question whether VGLL4 regulates
84 adipogenesis in vivo.
85 Previously, we generated a *Vgll4* mutant mouse allele, *Vgll4*^{d46}, in which a 46 bp deletion
86 caused a frameshift mutation and disrupted the TDU domain that mediates TEAD binding.
87 *Vgll4*$^{d46/d46}$ (*Vko*) mice could not prevail and died shortly after birth [26]. Using interscapular BAT
88 as a classical BAT example, here we show that *Vko* mice had much less BAT than their
89 littermate controls, and that VGLL4 is essential for the normal BAT adipogenesis gene
90 expression program. Additionally, overexpressing VGLL4 in postnatal BAT increased BAT
91 volume and protected the mice from acute cold stress. In summary, our study reveals that
92 VGLL4 is a crucial adipogenesis factor that controls BAT growth and function, thus advancing
93 the knowledge of BAT development.

94 ***Results***

95 ***Mutating VGLL4 causes BAT paucity.***

96 We have previously reported that whole-body depletion of VGLL4 led to perinatal death [26].
97 While characterizing the phenotype of the *Vgll4* knockout (*Vko*) pups, we noticed that the *Vko*

98 newborn pups had consistent dents in the interscapular regions, which led us to examine the
99 interscapular BAT depot. Impressively, the *Vko* pups had much smaller BAT depots than their
100 littermate controls (Fig. 1A). By performing qRT-PCR with the P0 BAT we confirmed the
101 depletion of *Vgll4* (Suppl. Fig. 1A).
102 To elucidate the cellular mechanism of BAT paucity, we first examined the BAC size and
103 found reduced BAC size in *Vko* compared with littermate controls (Suppl. Fig. 1B and 1C).
104 We then measured the proliferation rate of the UCP1-positive BACs with EdU, a thymidine
105 analogue that labels proliferating cells. *Vko* BACs had a comparable EdU incorporation rate to
106 controls (Suppl. Fig. 2D and 2E). Consistent with the malformation of BAT, the expression of
107 BAT marker UCP1 was reduced in the *Vko* mutants (Fig. 1B and 1C), suggesting that loss of
108 VGLL4 may either interfere with preadipocyte-to-BAC differentiation or impair BAC
109 maturation.
110 To determine if the BAT abnormalities preceded birth, we collected embryos at E18.5 and
111 examined the interscapular BAT depot. Compared with wild type controls, the *Vgll4*
112 heterozygous (*Vhet*) embryos had no obvious growth defects, as reflected by the normal body
113 weight (Suppl. Fig. 1F). The *Vko* mutants were smaller than both wild type and *Vhet* embryos;
114 however, the weight of the major internal organs, such as the heart and lungs, normalized to
115 body weight, was not affected (Suppl. Fig. 1G and 1H). Because we observed no phenotypic
116 difference between *Vhet* and wild type mice, we used both of these genotypes as controls. In
117 the control embryos, the interscapular regions were filled with BAT covered by white
118 adipocytes (Suppl. Fig. 1I); however, the *Vko* embryos had much smaller interscapular BAT
119 depots (Suppl. Fig. 1I), demonstrating that BAT paucity occurs in *Vko* during embryonic
120 development.
121 We further examined the BAT histology and lipid deposition in the neonatal *Vko* mutants.
122 The BAT depot was thinner in *Vko* than in controls (Fig. 1D, top row). The nuclei were more
123 dense in *Vko* BAT, and *Vko* BACs had less cytoplasmic vacuoles (Fig. 1D, bottom row).
124 Oil Red O staining revealed that lipid droplets were abundant in control BAT but rarely
125 detected in the *Vko* BAT (Fig. 1E), suggesting that VGLL4 is essential for BAT lipogenesis.
126 Similar to BAT, the inguinal subcutaneous white adipose tissue (iWAT) contained minimal
127 lipid droplets in *Vko*, whereas lipid droplets were readily detected in control iWAT (Fig. 1F).
128 Perilipin is a protein enriched on the surface of lipid droplets in differentiated adipocytes [27].
129 Compared with control iWAT, *Vko* iWAT had much less perilipin immunoreactivity (Fig. 1F). To
130 more broadly assess the effect of VGLL4 mutation on lipid deposition, we measured the lipid
131 composition of the chest and abdomen of control and *Vko* pups with magnetic resonance

132 imaging (MRI). Lipid signals were detected in the interscapular and subcutaneous regions of
133 control but not *Vko* pups (Fig. 1G). Quantification of the relative volume of BAT and
134 subcutaneous WAT revealed that both these adipose depots were much smaller in the *Vko*
135 pups (Fig. 1H and 1I). Additionally, quantification of the lipid signals contained in the chest and
136 abdomen tissues demonstrated a significant decrease of lipid content in the *Vko* mutants (Fig.
137 1J, *Vko* 1.49% vs Ctrl 19.59%, p=0.01). Together, these data suggest that VGLL4 regulates
138 adipogenesis in both BAT and subcutaneous WAT.

139 **Loss of VGLL4 disrupts the adipogenesis gene expression program of BAT.**

140 To determine whether VGLL4 inactivation changed the BAT gene expression program, we
141 performed RNA sequencing with BAT collected from P0 pups. Compared with littermate
142 controls, 1217 and 978 genes were significantly down- and up- regulated in the *Vko* BAT,
143 respectively (P_{adj}<0.05 and absolute FC>1.5; Fig. 2A, Dataset S1). Whole genome Gene Set
144 Enrichment Analysis (GESA) analysis [28] showed that myogenesis, oxidative phosphorylation,
145 fatty acid metabolism, and adipogenesis were the top four biological processes enriched in
146 the wild type BAT (Fig. 2B; Suppl. Fig.2A). Out of 191 genes in the adipogenesis gene set, 51
147 were down-regulated in *Vko* (Fig. 2C). We used qRT-PCR to validate the expression of *Acsl1,*
148 *Adipor2, Cidea* and *Dgat1,* and confirmed that all these genes except *Adipor2* were
149 decreased in *Vko* BAT (Fig. 2D).

150 To assess the BAC differentiation stage that is regulated by VGLL4, we took advantage of
151 published gene expression profiles of BACs at different stages of differentiation [29]. In this
152 study, 960 protein coding genes were found to be differentially expressed during pre-
153 adipocyte to BAC differentiation. Among these 960 genes, 856 genes were detected in our
154 RNA-seq data. Based on the expression data of these 856 genes, we performed hierarchical
155 clustering to determine which stage of differentiation was most similar to P0 control or *Vko*
156 BAT. Both the control and *Vko* BAT gene expression data clustered with that of the
157 differentiated BACs (Suppl. Fig. 2B), suggestive a minor role of VGLL4 during brown
158 preadipocyte to BAC differentiation.

159 We further measured the expression of two BAC-enriched genes (*Ucp1* and *Cox7a1*) and
160 two BAC differentiation-related genes (*Dlk1/Pref-1* and *Prdm16*). In comparison with control
161 BAT, *Vko* BAT had lower expression of *Ucp1* and *Cox7a1* (Fig. 2E) and similar expression of
162 *Dlk1* and *Prdm16* (Fig. 2F).

163 ***Deletion of VGLL4 activates IGF-Akt pathway.***

164 VGLL4 is a transcriptional regulator that blunts the interaction between YAP and TEAD
165 proteins [25]. It has been reported that mice doubly heterozygous for YAP and its paralog TAZ

166 had disrupted BAT growth, and that YAP/TAZ coordinated with TEAD1 to drive UCP1
167 expression in BACs [23]. These published data suggest that TEAD1 is involved in the
168 development of BAT. To test the correlation between TEAD1 expression and BAT
169 development, we examined *Tead1* mRNA and TEAD1 protein levels in the BAT at different
170 developmental stages. *Tead1* mRNA and TEAD1 protein were both high in postnatal day 1
171 (P1) BAT and then quickly decreased to a very low level at P4 (Fig. 3A; Suppl. Fig. 3A).
172 Different from *Tead1*, *Vgll4* mRNA level was decreased from P1 to P15 and then increased
173 from P15 to P30 (Supp. Fig. 3B).
174 We previously showed that activation of VGLL4 decreased TEAD1 protein level in the
175 heart [25] and knocking out VGLL4 increased TEAD1[26]. We then checked whether inactivation
176 of VGLL4 affected TEAD1 protein expression in BAT. Immunofluorescence staining showed
177 that TEAD1 expression and nuclear abundance was both increased in the BACs of neonatal
178 *Vko* (Fig. 3B). In line with these in situ observations, western blots confirmed that *Vko* BAT
179 had more TEAD1 than littermate controls (Fig. 3C and 3D). The YAP/TEAD complex regulates
180 the expression of IGFR-Akt pathway components [30,31]. Consistent with the upregulation of
181 TEAD1, the *Vko* pups had increased IGF1R and higher phospho Akt/Akt ratio (Fig. 3C and
182 3D). These data suggest that VGLL4 ablation increases the transcriptional activity of the
183 TEAD1/YAP complex in BAT.
184 Next, we measured the protein levels of PPAR-γ and CEBPβ, two transcriptional factors
185 central to the regulation of adipogenesis [32,33]. PPARγ was significantly increased in *Vko* BAT
186 (Fig. 3E and 3F), suggesting that loss of VGLL4 does not impair BAT adipogenesis by
187 decreasing PPARγ expression. CEBPβ plays a central role in adipocyte differentiation [33], and
188 it has several N-terminally truncated isoforms, such as liver-enriched activator protein (LAP)
189 and liver-enriched inhibitory protein (LIP). CEBPβ-LAP interacts with PRDM16 to direct the
190 differentiation of myoblastic precursors into BACs [34], and CEBPβ-LIP rescued the growth
191 defects of *Cebpb* knockout mice [35], suggesting that CEBP-LIP and CEBP-LAP have
192 overlapping functions. Compared to control BAT, CEBPβ-LAP expression in *Vko* BAT was
193 similar, but CEBPβ-LIP was significantly lower (Fig. 3E and 3F).
194 Adipose triglyceride lipase (ATGL) is a well-known lipolysis enzyme and highly
195 expressed in the adipose tissues of mice and humans [36]. It recently was shown to regulate the
196 synthesis of branched fatty acid esters of hydroxy fatty acids (FAHFAs) [37], a class of newly
197 discovered lipids that have favorable metabolic and anti-inflammatory effects [38]. In *Vko* BAT,
198 ATGL expression was very low compared to control BAT (Fig. 3E and 3F), further suggesting
199 that loss of VGLL4 impairs the development of BAT.

VGLL4/TEAD1 complex regulates the expression of BAT myogenesis genes.

We suspected that VGLL4 might interact with TEAD1 to regulate BAC gene expression. To test this hypothesis, we used a genomic approach to identify the genes that are regulated by both VGLL4 and TEAD1.

Because TEAD1 expression was high in the young newborn pups (Fig. 3A), we used P0 BAT to identify genes directly bound by TEAD1 using TEAD1 chromatin immunoprecipitation followed by next generation sequencing (ChIP seq). *Tead1*^{fb} knockin mice that express FLAG and BIO epitope tagged TEAD1 [25] were crossed to BirA transgenic mice [39] to generate *Tead1*^{fb};*BirA* mice, in which the endogenous TEAD1^{fb} protein was biotylated by BirA.

TEAD1 bioChIP-seq of P0 *Tead1*^{fb}*;BirA* BAT revealed 4234 peaks that mapped to 2834 genes, with 371 peaks localized in the promoter region (0 to -5kb upstream of the transcriptional starting site), and the rest of the peaks spreading out in the gene bodies and distal noncoding regions (Suppl. Fig. 4A). De novo motif discovery [40] identified the TEAD binding motif as the mostly enriched motif (Fig. 4A), thus confirming the reliability of our ChIP seq data set. The other top five transcriptional factors that were co-enriched in the TEAD1 ChIP peaks were Nuclear factor 1 (NF1), CCCTC-Binding Factor (CTCF), CEBP, Early B Cell Factor transcription factor 1 (EBF1) and Myocyte Enhancer Factor 2C (MEF2c) (Fig. 4A). Among these five transcriptional factors, both NF1 and CEBP protein families are essential for BAT adipogenesis [14,41], suggesting that TEAD1 may coordinate with these transcriptional factors to regulate BAT development.

Pathway analysis with the 2834 TEAD1-bound genes showed that the Hippo signaling pathway was among the top five enriched pathways (Fig. 4B). By comparing the *Vko* BAT differentially regulated genes (DEG) with the TEAD1-bound genes, we identified 419 overlapped genes that might be directly regulated by VGLL4 and TEAD1 (Fig. 4C). Gene ontology term analysis [42] of these 419 genes revealed that muscle structure development was the most enriched biological process (Fig. 4D). 37 TEAD1-bound genes were differentially expressed in *Vko* BAT and related to muscle structure development (Fig. 4E). Myogenic gene expression is a molecular signature that separates BACs from white adipocytes [43]. These data suggest that the VGLL4/TEAD1 complex regulates the expression of myogenic genes in BAT.

In addition to regulating myogenic genes, TEAD1 also bound to crucial lipogenesis genes, such as *Fabp4, Lpl, Fabp3, Cd36, Prdm16, Cav1, Slc27a1,* and *Ppargc1b* (Suppl. Fig. 4B). qRT-PCR tests confirmed that *Cav1*, *Fabp3*, *Slc27a1,* and *Ppargc1b* were all down regulated in the *Vko* BAT (Suppl. Fig. 4C).

VGLL4 alleviates TEAD1 suppression of CEBPβ transcriptional activity.

234 Calsequestrin1 (*Casq1*) encodes a high-capacity calcium-binding protein that acts as a
235 Ca^{2+} storage/buffer molecule in the sarcoplasmic reticulum of skeletal muscle cells [44]. *Casq1*
236 is also expressed in BAT, and down regulation of *Casq1* is associated with decreased BAT
237 thermogenic capacity [45]. Unbiased *Vko* BAT gene expression profiling and TEAD1 ChIP-seq
238 analysis identified *Casq1* as a direct target of the VGLL4/TEAD1 complex (Fig. 4E). As shown
239 in Fig. 5A, TEAD1 directly bound to the promoter region of *Casq1*. In BAT, *Vgll4* inactivation
240 robustly decreased *Casq1* mRNA (Fig. 5B). TEAD1 ChIP-seq peak region encompassed 480
241 base pairs (bp) of the *Casq1* promoter. Analysis of mouse and human sequences using the
242 evolutionary conserved regions (ECR) genome browser [46] showed that the sequence is highly
243 conserved (Fig. 5C) and contains one CEBP binding motif and one TEAD1 binding motif, both
244 of which were identical between mouse and human (Fig. 5D).
245 To study the activity of murine *Casq1* promoter, we constructed Casq1-Luci, in which the
246 480 bp TEAD1-bound region was positioned upstream of the luciferase gene in the
247 promoterless pGL2 basic vector (Fig. 5E). In HEK293T cells, CEBPβ increased Casq1-Luci
248 reporter activity, which was attenuated by further addition of TEAD1. VGLL4 did not affect
249 CEBPβ transcriptional activity, but it abolished TEAD1 suppression of CEBPβ (Fig. 5E).
250 We performed co-immunoprecipitation (Co-IP) assays in HEK293T cells to characterize
251 the relationships between CEBPβ, VGLL4, and TEAD1. Plasmids expressing TEAD1-HA,
252 VGLL4-GFP and CEBPB-FLAG were co-transfected into HEK293T cells in different
253 combinations. In the absence of TEAD1-HA, CEBPβ-FLAG pulled down VGLL4-GFP (Suppl.
254 Fig.5); in the absence of VGLL4-GFP, CEBPβ-FLAG pulled down TEAD1-HA (Fig. 5F). When
255 these three proteins were co-expressed in HEK293T cells, CEBPβ pulled down both VGLL4
256 and TEAD1 (Fig. 5F). These data suggest that TEAD1 and VGLL4 each bind to CEBPβ in a
257 non-exclusive manner.
258 Altogether, these data suggest that TEAD1 suppresses CEBPβ activation of *Casq1*
259 expression, and that VGLL4 favors *Casq1* expression by abolishing TEAD1 suppression of
260 CEBPβ.
261 **Construction and validation of a BAC-specific AAV construct.**
262 AAV-mediated transduction of adipose tissue is a convenient tool for studying adipose
263 pathophysiology, and AAV serotype 9 has a very high transduction efficiency for BAT [47]. To
264 facilitate gene-function studies in BAT, we generated a new AAV construct in which brown
265 adipose tissue-specific cis-regulatory elements (BCE) derived from murine *Ucp1* drive cargo
266 gene expression (Suppl. Fig. 6). To test the specificity and activity of BCE, we cloned either
267 luciferase or GFP into this construct (Fig. 6A). 3-day-old pups (P3) were treated with

268 AAV9.BCE.Luci and AAV9.BCE.GFP. 6 weeks post AAV delivery, we examined the tissue
269 specificity of these AAV constructs (Fig. 6B). In vivo bioluminescence imaging showed that
270 luciferase activity was limited to the interscapular region (Fig. 6C). Overlay of the luciferase
271 signal onto whole animal microCT data confirmed that it originated from BAT (Fig. 6D).
272 Histological sections of interscapular adipose tissue confirmed that BCE-driven GFP was
273 expressed in BACs and not in the adjacent white adipocytes (Fig. 6E).

274 **Overexpressing VGLL4 in BACs promotes BAT growth.**

275 Because loss of VGLL4 caused BAT paucity (Fig. 1), we asked whether overexpressing
276 VGLL4 in BACs promotes BAT growth.

277 To answer this question we generated AAV.BCE.VGLL4^{GFP} (BCE.VGLL4^{GFP}), in which
278 BAC-specific BCE regulatory elements drive the expression of GFP tagged human VGLL4.
279 We treated p3 pups with BCE.VGLL4^{GFP} and assessed BAT volume at P42 using microCT
280 (Fig. 7A). BCE.GFP was used as a control. Compared with BCE.GFP treated mice,
281 BCE.VGLL4^{GFP} mice showed significantly higher BAT volume (102.20 ± 2.77 vs 84.16 ± 1.86
282 mm^3, Fig. 7B), whereas the body weight of these two cohorts animals was not distinguishable
283 (Fig. 7C). Consistent with the *microCT* measurements, the BAT weight to body weight ratio
284 was significantly higher for BCE.VGLL4^{GFP} compared to BCE.GFP (Fig. 7D).

285 We collected the BAT tissue to confirm the expression of VGLL4^{GFP}. Western blot
286 detected the expression of VGLL4^{GFP} in the BCE.VGLL4^{GFP} transduced mice (Fig. 7E), and in
287 situ immunofluorescence staining showed that VGLL4^{GFP} signals were enriched in the nuclei
288 of BACs (Suppl. Fig. 7A).

289 Because lipogenesis-driven BAC enlargement is one of the underlying mechanisms of
290 postnatal BAT growth [11], we suspected that VGLL4 might promote BAT growth by increasing
291 BAC size. We tested this hypothesis by staining BAT sections with Phalloidin, which labels the
292 filamentous actin cytoskeleton [48]. Compared to BCE.GFP, BCE.VGLL4^{GFP} significantly
293 increased BAC size (Suppl. Fig. 7B and 7C), which was associated with the increase of lipid
294 content as visualized by BODIPY (a neutral lipid dye) staining (Suppl. Fig. 7D and 7E). To
295 corroborate the in vivo results, we overexpressed VGLL4 in an immortalized brown
296 preadipocyte (IBA) cell line [29] and tested VGLL4's adiogenetic effects. Compared with GFP
297 control, VGLL4 promoted lipid deposition in differentiated IBA cells (Suppl. Fig. 7F).
298 Correspondingly, qRT-PCR results demonstrated the robust increase of three lipogenesis
299 genes: *Fasn*, *Cidea* and *Acsl1* (Suppl. Fig. 7G). Thus, our in vitro and in vivo data strongly
300 suggest that activation of VGLL4 promotes BAT growth by increasing BAC lipogenesis.

301 Thermogenesis is one of the biological functions of BAT. We asked whether activating

302 VGLL4 in BAT affected whole body thermogenesis. To address this issue, we transduced P3
303 wild type mouse pups with BCE.VGLL4^{GFP} and performed acute cold stress test 6 weeks post
304 AAV transduction. Age-matched BCE.GFP transduced mice were used as control.
305 BCE.VGLL4^{GFP} and BCE.GFP mice were applied to acute 4°C cold stress for 24 hours. The
306 core temperature of these two cohorts of mice were indistinguishable under regular housing
307 temperature (~22 °C). In the first 20-hour acute cold stress period, the core temperature of
308 male BCE.GFP mice decreased from 37.10 $\pm$ 0.21 °C to 35.28 $\pm$ 0.72 °C; however, the core
309 temperature of the male BCE.VGLL4^{GFP} mice did not change (37.43 $\pm$ 1.15 vs 37.80 $\pm$ 0.62)
310 (Fig. 7F). In contrast to the male mice, the female mice did not show a core temperature
311 difference between BCE.GFP and BCE.VGLL4^{GFP} groups (Fig. 7G).

312 On the molecular level, we collected BAT after acute cold stress and measured the
313 expression of several VGLL4/TEAD1 target genes, including *Casq1, Myh9, Smad6,* and
314 *Tpm1.* qRT-PCR results showed that VGLL4 increased *Casq1* and decreased *Smad6* (Fig.
315 7H). In line with our observation that VGLL4 promoted lipogenesis, *Cidea* expression was
316 increased in BCE.VGLL4^{GFP} BAT. Although VGLL4 activation increased BAT thermogenesis,
317 we found that VGLL4 decreased *Ucp1* expression, rather than increasing it (Fig. 7H).

318 **Discussion**

319 In this study, we found that germ-line deletion of the VGLL4 TDU domains impaired BAT
320 growth. Our data suggest that BAT adipogenesis requires VGLL4.

321 From fetus to early life, the development of BACs encompasses four stages: 1)
322 mesenchymal stem cells differentiate into myogenic factor 5 (Myf5)-expressing progenitor
323 cells; 2) Myf5^{+} progenitor cells differentiate into brown preadipocytes; 3) preadipocytes
324 differentiate into UCP1-positive naive BACs; 4) naive BACs develop into lipid-loaded and
325 mitochondria abundant mature BACs [9]. Our current data advocate the hypothesis that VGLL4
326 regulates BAT growth by orchestrating molecular events that occur between stage 3 and 4, a
327 developmental period required for brown preadipocytes turning into lipid-loaded and
328 thermogenesis active mature BACs. This hypothesis is supported by the following data sets:
329 first, loss of VGLL4 impairs BAC lipogenesis and UCP1 expression; second, the *Vko* BAT
330 gene expression signature was more similar to the differentiated BACs than the
331 undifferentiated brown preadipocytes; third, VGLL4 gain-of-function studies show that
332 activating VGLL4 increased BAT volume and BAC size; fourth, VGLL4 promotes lipogenesis
333 in cultured BACs.

334 We found that VGLL4 promotes both BAT and WAT lipogenesis *in vivo*. This result differs
335 from studies performed in cultured 3T3L1 cells, which suggested that VGLL4 suppresses

336 adipogenesis [22]. One possibility is that under physiological conditions, VGLL4 is essential for
337 orchestrating the lipogenesis of adipocytes. However, under harsh chemical adipogenesis
338 conditions, such as the chemical cocktail for inducing 3T3L1 cells differentiation into
339 adipocytes, VGLL4 may be required to block the excessive activity of the adipogenesis
340 factors.

341 Akt signaling is pivotal for BAT development, because genetically ablation of Akt1 and
342 Akt2 severely diminished BAT growth [49]. In the neonatal *Vko* BAT, the expression of TEAD1,
343 IGFR and phospho-Akt were all increased, suggestive of VGLL4 impairing BAT development
344 without blunting Akt pathway. PPARγ and CEBPβ are two master regulators of adipogenesis
345 [13,14,50]. In rodents, CEBPβ-LIP is abundant in fetal BAT and low in adult BAT [51], and expressing
346 CEBPβ-LIP in the CEBPβ knockout mice rescued BAT adipogenesis [35], implying that CEBPβ-
347 LIP is critical for BAT development. In *Vko* BAT, PPARγ was increased, whereas the
348 expression of two CEBPβ isoforms was differentially regulated, with the larger CEBPβ-LAP
349 isoform remaining unchanged and the smaller CEBPβ-LIP isoform being substantially
350 reduced.

351 As VGLL4's partner and one of the terminal effectors of Hippo-YAP pathway, TEAD1 is
352 highly expressed in the P1 BAT and its expression decreases with age. In P0 BAT, TEAD1
353 bound regions are enriched with CEBP binding motif, suggestive of TEAD1 and CEBP
354 collaborative binding. Using the murine *Casq1* promoter that contains conserved TEAD1 and
355 CEBP binding motifs as a probe, we found that CEBPβ activated *Casq1* expression whereas
356 adding in TEAD1 weakened CEBPβ's transcriptional activity. This TEAD1 suppression of
357 CEBPβ is likely a direct regulation due to direct protein-protein interactions, because co-IP
358 experiments indicate that these proteins interact with each other. VGLL4 is known to
359 physically interact with TEAD1, and here we show that VGLL4 also interacts with CEBPβ.
360 Although VGLL4 did not affect CEBPβ transcriptional activity, it abolished TEAD1 suppression
361 of CEBPβ. The discovery of VGLL4 alleviating TEAD1 suppression of CEBPβ, together with
362 the aforementioned *Vko* BAT signaling pathways profiling data suggest that VGLL4 and
363 TEAD1 are bridge molecules connecting Hippo-YAP pathway with CEBPβ, one of the core
364 adipogenesis regulators.

365 YAP/TAZ, TEADs and VGLLs are three categories of crucial transcriptional effectors of
366 the Hippo-YAP pathway. YAP/TAZ interacts with TEADs to regulate target gene expression,
367 and VGLLs function as suppressors of YAP/TEAD1 complex by competing for TEAD [24].
368 Published data show that YAP and TAZ suppress BAT lipogenesis, because reducing YAP
369 and TAZ expression in BAT robustly increased BAC lipid content. In the same work, YAP and

370 TAZ were found to serve as mechanosensor proteins in BAT to regulate BAC thermogenesis.
371 Mechanistically, adrenergic stimulation increases cytosolic Ca^{2+} that activates actomyosin
372 machinery to cause cellular tension, which in turn increases *Ucp1* expression by activating
373 YAP/TAZ-TEAD complex [23]. In the current study, our data suggest that VGLL4 has dual roles
374 in the regulation of BAT development: during embryo development, VGLL4 is required for
375 brown preadipocytes differentiating into UCP1 positive brown adipocytes and may regulate
376 adipogenesis by preserving CEBPβ transcriptional activity; from neonate to adulthood, VGLL4
377 favors lipogenesis and suppresses *Ucp1* expression, and VGLL4 fulfills this function by
378 competing against YAP/TAZ for limited TEAD proteins.
379 Although UCP1-dependent energy dissipation is critical for BAT thermogenesis [52], it is
380 not the only molecular mechanism for BAT to generate heat. UCP1-independent energy
381 dissipation molecular mechanisms, such as Ryr1-mediated Ca^{2+} leak [53], also contribute to
382 BAT thermogenesis. Different from YAP/TAZ promoting BAT thermogenesis by increasing
383 UCP1 expression, VGLL4 induction of adult BAT thermogenesis is associated with *Ucp1*
384 down-regulation, thus suggesting that VGLL4 increases BAT thermogenesis by activating
385 UCP1-independent energy dissipation mechanisms. Since *Casq1* encodes a Ca^{2+} buffer
386 protein and it is up-regulated by VGLL4, future studies are required to test whether VGLL4
387 promotes thermogenesis through activating futile Ca^{2+} recycling [54].
388 In conclusion, our data suggest that Hippo-YAP pathway terminal effector proteins (e.g.,
389 TEAD1 and VGLL4) regulate BAT adipogenesis through modulating the transcriptional activity
390 of CEBPβ, thus improving our understanding of how Hippo-YAP pathway regulates BAT
391 development and function.

392 **Materials and Methods**

393 Refer to the Supplemental Information for Extended Materials and Methods.

394 *Mice*

395 All animal procedures were approved by the Institutional Animal Care and Use
396 Committee of the Masonic Medical Research Institute. Wild type C57/BL6J mice were used in
397 this study. C57/BL6J mice were originally purchased from Jackson Laboratory and maintained
398 in the AAALAC accredited (#001865) mouse facility of Masonic Medical Research Institute
399 (MMRI). *Vgll4* knockout mouse line [26], *Tead1*^{fb} knockin [25] and BirA mouse lines were
400 published previously [39].

401 *Statistics*

402 Data values (e.g., gene and protein expression data) were expressed as mean ± SD.
403 Normally distributed data were analyzed with student's t-test (two groups) or one-way ANOVA

404 followed by Tukey's post hoc test (more than two groups). Non-parametric data (e.g., cell
405 size) were analyzed using Mann-Whitney test (two groups). Prism10 software was used to
406 plot the bar/violin graphs and to perform the statistical analysis.

407 **Data availability**

408 TEAD1 bioChIP-seq data of postnatal day 0 (P0) mouse brown adipose tissue has been
409 deposited to gene expression omnibus GSE271532. Bulk RNA-seq data of wildtype and Vgll4
410 knockout P0 mouse brown adipose tissue has been deposited to GSE271533.

411 **Sources of Funding**

412 Z. Lin was supported by AHA Scientist Development Grant 15SDG25590001, NIH
413 HL138454-01, and 1R01HL146810. W.T. Pu was supported by NIH R01HL116461 and
414 R01HL146634.

415 **Author contributions:** Z.L. designed and interpreted the study. P.Z., C.W.K. and Z.L. per-
416 formed experiments with the help from A.D., G. W., J.S.K. and S.N.. F. G. analyzed the BAT
417 RNA-seq data. B. D. provided the IBA RNA-seq data and IBA cell line. P. Z., C.W.K. W.T. P
418 and Z. L analyzed the results. Z.L wrote the manuscript. C.W.K. and W.T. P. revised the
419 manuscript.

420 **Acknowledgment:** We thank Jimiao Sun from Boston Children's Hospital for quantifying the
421 mouse pups lipid content with the magnetic resonance imaging (MRI) data.

422 **Disclosures.** Z.L. holds a patent (Patent No. US 11,319, 354 B2) that is related with the cur-
423 rent study.

References:

1. Mitchell, N. S., Catenacci, V. A., Wyatt, H. R. & Hill, J. O. Obesity: overview of an epidemic. *Psychiatr Clin North Am* **34**, 717-732 (2011).

2. Zwick, R. K., Guerrero-Juarez, C. F., Horsley, V. & Plikus, M. V. Anatomical, Physiological, and Functional Diversity of Adipose Tissue. *Cell Metab* **27**, 68-83 (2018).

3. Symonds, M. E. Brown adipose tissue growth and development. *Scientifica (Cairo)* **2013**, 305763 (2013).

4. Giralt, M. & Villarroya, F. White, brown, beige/brite: different adipose cells for different functions. *Endocrinology* **154**, 2992-3000 (2013).

5. Heaton, J. M. The distribution of brown adipose tissue in the human. *J Anat* **112**, 35-39 (1972).

6. Cypess, A. M. et al. Identification and importance of brown adipose tissue in adult humans. *N Engl J Med* **360**, 1509-1517 (2009).

7. Cypess, A. M. & Kahn, C. R. Brown fat as a therapy for obesity and diabetes. *Curr Opin Endocrinol Diabetes Obes* **17**, 143-149 (2010).

8. Gesta, S., Tseng, Y. H. & Kahn, C. R. Developmental origin of fat: tracking obesity to its source. *Cell* **131**, 242-256 (2007).

9. Yao, X., Shan, S., Zhang, Y. & Ying, H. Recent progress in the study of brown adipose tissue. *Cell Biosci* **1**, 35 (2011).

10. Schulz, T. J. et al. Brown-fat paucity due to impaired BMP signalling induces compensatory browning of white fat. *Nature* **495**, 379-383 (2013).

11. Negron, S. G., Ercan-Sencicek, A. G., Freed, J., Walters, M. & Lin, Z. Both proliferation and lipogenesis of brown adipocytes contribute to postnatal brown adipose tissue growth in mice. *Sci Rep* **10**, 20335 (2020).

12. Townsend, K. & Tseng, Y. H. Brown adipose tissue: Recent insights into development, metabolic function and therapeutic potential. *Adipocyte* **1**, 13-24 (2012).

13. Jones, J. R. et al. Deletion of PPARgamma in adipose tissues of mice protects against high fat diet-induced obesity and insulin resistance. *Proc Natl Acad Sci U S A* **102**, 6207-6212 (2005).

14. Tanaka, T., Yoshida, N., Kishimoto, T. & Akira, S. Defective adipocyte differentiation in mice lacking the C/EBPbeta and/or C/EBPdelta gene. *EMBO J* **16**, 7432-7443 (1997).

15. Seale, P. et al. Transcriptional control of brown fat determination by PRDM16. *Cell Metab* **6**, 38-54 (2007).

16. Pan, D. The hippo signaling pathway in development and cancer. *Dev Cell* **19**, 491-505 (2010).

17. Meng, Z., Moroishi, T. & Guan, K. L. Mechanisms of Hippo pathway regulation. *Genes Dev* **30**, 1-17 (2016).

18. Morrison, S. & McGee, S. L. 3T3-L1 adipocytes display phenotypic characteristics of multiple adipocyte lineages. *Adipocyte* **4**, 295-302 (2015).

19. Park, B. H. et al. Mammalian ste20-like kinase and SAV1 promote 3T3-L1 adipocyte differentiation by activation of PPARγ. *PLoS One* **7**, e30983 (2012).

20. An, Y., Kang, Q., Zhao, Y., Hu, X. & Li, N. Lats2 modulates adipocyte proliferation and

466 differentiation via hippo signaling. *PLoS One* **8**, e72042 (2013).

467 21. Yu, F. X. et al. Protein kinase A activates the Hippo pathway to modulate cell prolifera-
468 tion and differentiation. *Genes Dev* **27**, 1223-1232 (2013).

469 22. Zhang, W. et al. The TEA domain family transcription factor TEAD4 represses murine
470 adipogenesis by recruiting the cofactors VGLL4 and CtBP2 into a transcriptional complex. *J*
471 *Biol Chem* **293**, 17119-17134 (2018).

472 23. Tharp, K. M. et al. Actomyosin-Mediated Tension Orchestrates Uncoupled Respiration
473 in Adipose Tissues. *Cell Metab* **27**, 602-615.e4 (2018).

474 24. Koontz, L. M. et al. The Hippo effector Yorkie controls normal tissue growth by antago-
475 nizing scalloped-mediated default repression. *Dev Cell* **25**, 388-401 (2013).

476 25. Lin, Z. et al. Acetylation of VGLL4 Regulates Hippo-YAP Signaling and Postnatal Car-
477 diac Growth. *Dev Cell* **39**, 466-479 (2016).

478 26. Sheldon, C., Farley, A., Ma, Q., Pu, W. T. & Lin, Z. Depletion of VGLL4 Causes Perina-
479 tal Lethality without Affecting Myocardial Development. *Cells* **11**, 2832 (2022).

480 27. Greenberg, A. S. et al. Perilipin, a major hormonally regulated adipocyte-specific phos-
481 phoprotein associated with the periphery of lipid storage droplets. *J Biol Chem* **266**,
482 11341-11346 (1991).

483 28. Subramanian, A. et al. Gene set enrichment analysis: a knowledge-based approach for
484 interpreting genome-wide expression profiles. *Proc Natl Acad Sci U S A* **102**, 15545-15550
485 (2005).

486 29. Pradhan, R. N. et al. Dissecting the brown adipogenic regulatory network using integra-
487 tive genomics. *Sci Rep* **7**, 42130 (2017).

488 30. Lin, Z. et al. Pi3kcb links Hippo-YAP and PI3K-AKT signaling pathways to promote car-
489 diomyocyte proliferation and survival. *Circ Res* **116**, 35-45 (2015).

490 31. Xin, M. et al. Regulation of insulin-like growth factor signaling by Yap governs car-
491 diomyocyte proliferation and embryonic heart size. *Sci Signal* **4**, ra70 (2011).

492 32. Farmer, S. R. Transcriptional control of adipocyte formation. *Cell Metab* **4**, 263-273
493 (2006).

494 33. Guo, L., Li, X. & Tang, Q. Q. Transcriptional regulation of adipocyte differentiation: a
495 central role for CCAAT/enhancer-binding protein (C/EBP) β. *J Biol Chem* **290**, 755-761
496 (2015).

497 34. Seale, P., Kajimura, S. & Spiegelman, B. M. Transcriptional control of brown adipocyte
498 development and physiological function--of mice and men. *Genes Dev* **23**, 788-797 (2009).

499 35. Bégay, V., Baumeier, C., Zimmermann, K., Heuser, A. & Leutz, A. The C/EBPβ LIP
500 isoform rescues loss of C/EBPβ function in the mouse. *Sci Rep* **8**, 8417 (2018).

501 36. Zimmermann, R. et al. Fat mobilization in adipose tissue is promoted by adipose
502 triglyceride lipase. *Science* **306**, 1383-1386 (2004).

503 37. Patel, R. et al. ATGL is a biosynthetic enzyme for fatty acid esters of hydroxy fatty
504 acids. *Nature* **606**, 968-975 (2022).

505 38. Yore, M. M. et al. Discovery of a class of endogenous mammalian lipids with anti-dia-
506 betic and anti-inflammatory effects. *Cell* **159**, 318-332 (2014).

507 39. Driegen, S. et al. A generic tool for biotinylation of tagged proteins in transgenic mice.

Transgenic research **14**, 477-482 (2005).

40. Heinz, S. et al. Simple combinations of lineage-determining transcription factors prime cis-regulatory elements required for macrophage and B cell identities. *Mol Cell* **38**, 576-589 (2010).

41. Hiraike, Y. et al. NFIA co-localizes with PPARγ and transcriptionally controls the brown fat gene program. *Nat Cell Biol* **19**, 1081-1092 (2017).

42. Ge, S. X., Jung, D. & Yao, R. ShinyGO: a graphical gene-set enrichment tool for animals and plants. *Bioinformatics* **36**, 2628-2629 (2020).

43. Timmons, J. A. et al. Myogenic gene expression signature establishes that brown and white adipocytes originate from distinct cell lineages. *Proc Natl Acad Sci U S A* **104**, 4401-4406 (2007).

44. Sanchez, E. J., Lewis, K. M., Danna, B. R. & Kang, C. High-capacity Ca2+ binding of human skeletal calsequestrin. *J Biol Chem* **287**, 11592-11601 (2012).

45. Anthony, S. R. et al. HuR expression in adipose tissue mediates energy expenditure and acute thermogenesis independent of UCP1 expression. *Adipocyte* **9**, 335-345 (2020).

46. Ovcharenko, I., Nobrega, M. A., Loots, G. G. & Stubbs, L. ECR Browser: a tool for visualizing and accessing data from comparisons of multiple vertebrate genomes. *Nucleic Acids Res* **32**, W280-6 (2004).

47. Jimenez, V. et al. In vivo adeno-associated viral vector-mediated genetic engineering of white and brown adipose tissue in adult mice. *Diabetes* **62**, 4012-4022 (2013).

48. Kim, J. I. et al. During Adipocyte Remodeling, Lipid Droplet Configurations Regulate Insulin Sensitivity through F-Actin and G-Actin Reorganization. *Mol Cell Biol* **39**, e00210-19 (2019).

49. Shearin, A. L., Monks, B. R., Seale, P. & Birnbaum, M. J. Lack of AKT in adipocytes causes severe lipodystrophy. *Molecular metabolism* **5**, 472-479 (2016).

50. Xiong, W. et al. Brown adipocyte-specific PPARγ (peroxisome proliferator-activated receptor γ) deletion impairs perivascular adipose tissue development and enhances atherosclerosis in mice. *Arteriosclerosis, thrombosis, and vascular biology* **38**, 1738-1747 (2018).

51. Manchado, C. et al. CCAAT/enhancer-binding proteins α and β in brown adipose tissue: evidence for a tissue-specific pattern of expression during development. *Biochemical Journal* **302**, 695-700 (1994).

52. Fedorenko, A., Lishko, P. V. & Kirichok, Y. Mechanism of fatty-acid-dependent UCP1 uncoupling in brown fat mitochondria. *Cell* **151**, 400-413 (2012).

53. Bal, N. C. et al. Sarcolipin is a newly identified regulator of muscle-based thermogenesis in mammals. *Nature medicine* **18**, 1575-1579 (2012).

54. Guarnieri, A. R., Benson, T. W. & Tranter, M. Calcium cycling as a mediator of thermogenic metabolism in adipose tissue. *Mol Pharmacol* **102**, 51-59 (2022).

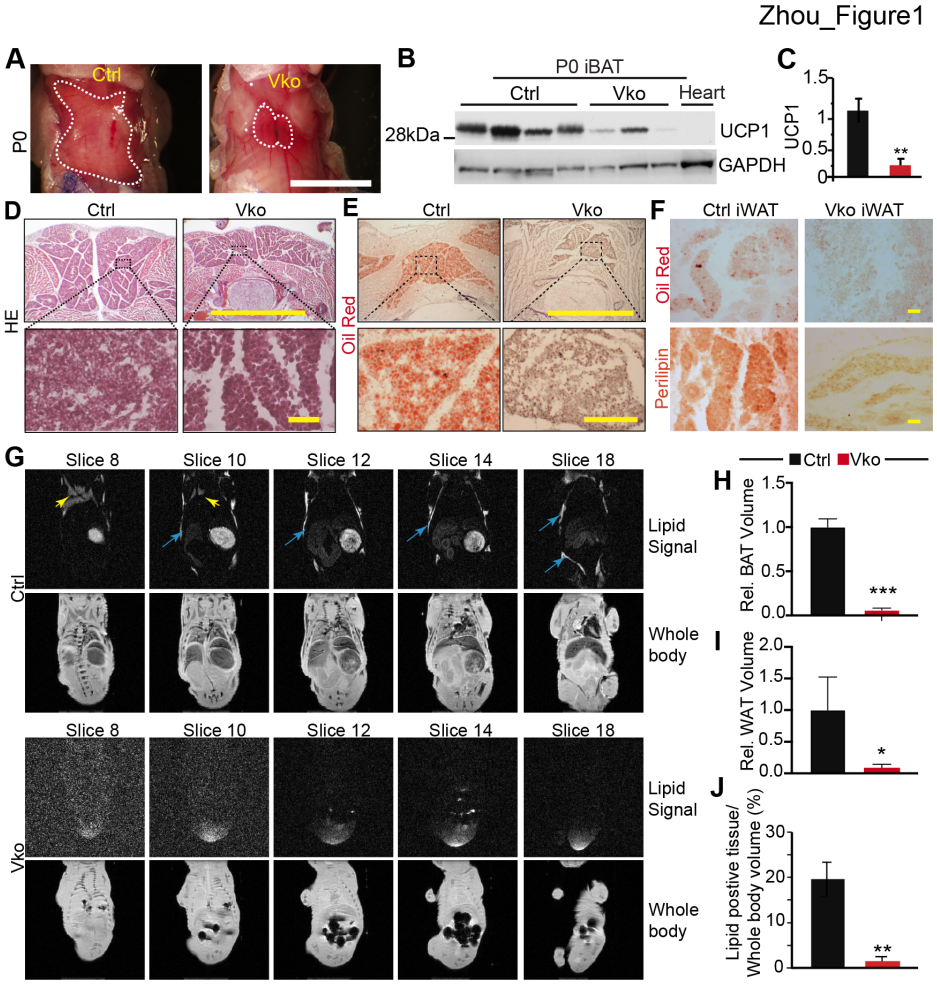

Figure 1. Classical brown adipose tissue growth requires VGLL4.

A. Gross morphology of classical interscapular brown adipose tissue at P0. Dotted lines indicate the BAT depot. Scale bar=4 mm. **B**. UCP1 immunoblot with P0 BAT protein. Heart protein was used as negative control. **C**. Densitometry quantification of UCP1. Protein levels were normalized to GAPDH. N=4. Student's t test, **, P<0.01. **D**. HE staining of BAT. Top panel, scale bar =4 mm; bottom panel, scale bar=50 μm. **E.** Oil Red O staining of BAT. Top panel, bar= 4 mm; bottom panel, scale bar=1 mm. **F.** Oil Red O staining and Perilipin immunohistological staining of iWAT. Scale bar = 50 μm **G**. Visualization of whole body trunk for lipid content by a series of MRI images using P0 mouse pups. Water signal was suppressed in the lipid only images. Blue and yellow arrows indicate BAT and and subcutaneous WAT, respectively. **H.** BAT lipid content comparison. **I**. WAT lipid content comparison. **J**. Quantification of the total lipid content. The percentage was calculated by normalizing the lipid positive tissue volume to the body trunk volume. Student t-test: *P<0.05, n=4.

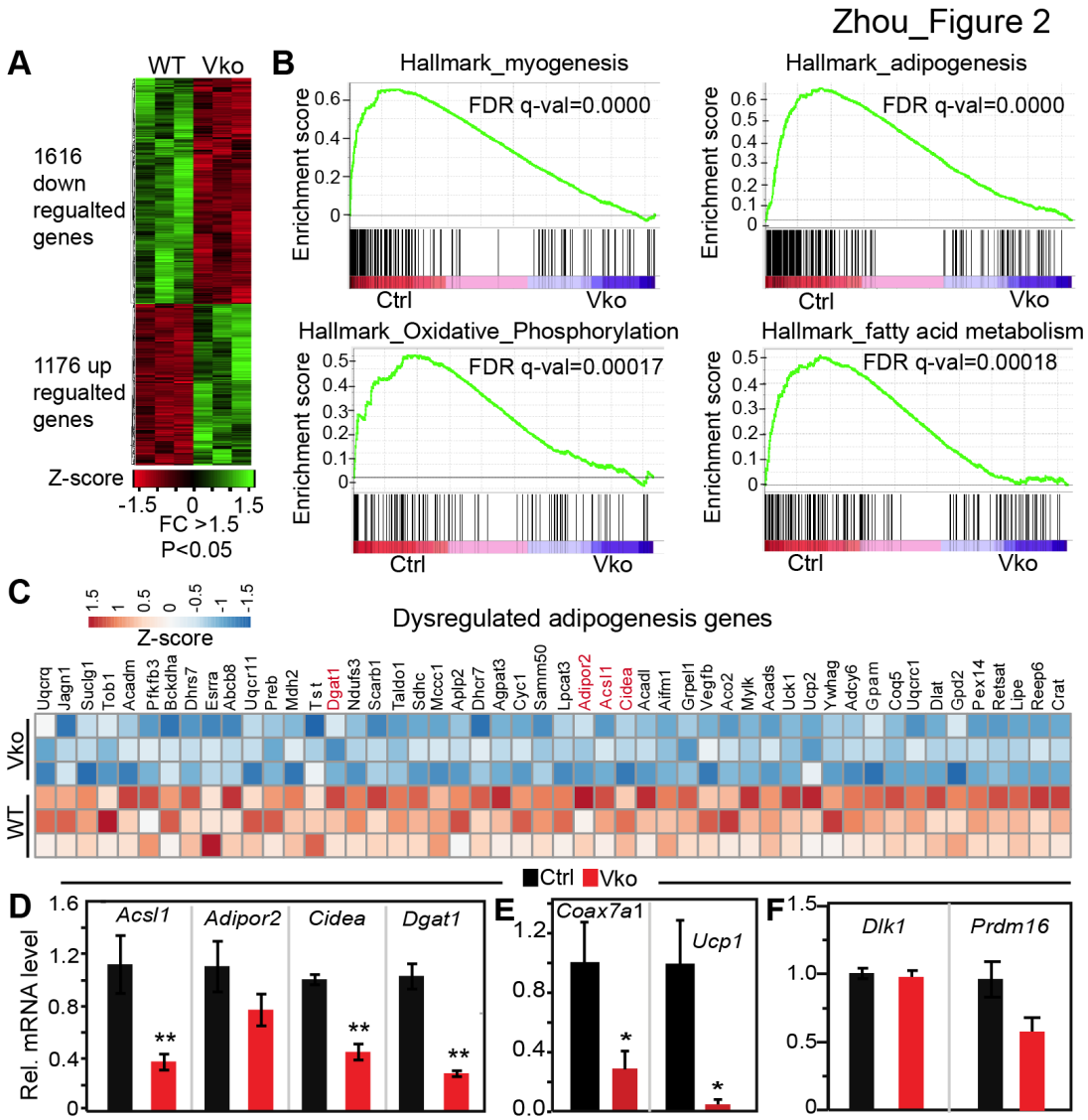

Figure 2. Loss of VGLL4 disrupts the adipogenesis gene expression program of BAT. **A**. Heat map of differentially expressed genes (DEG). RNA sequencing data from P0 BAT was analyzed with Deseq. N=3. **B**. Gene set enrichment analysis (GESA). GESA was carried out with the Deseq2-derived gene expression data set. The top four gene sets enriched in wild-type BAT were shown. **C**. A heat map of differentially expressed fatty acid metabolism/ adipogenesis genes. **D**. qRT-PCR validation of selected lipogenesis genes dysregulated in *Vko* BAT. **E-F.** qRT-PCR measurement of brown adipocyte differentiation-related genes. D, E and F, N=5. Student t-test, *, P<0.05. All the tested mRNAs were normalized by endogenous 36B4 mRNA.

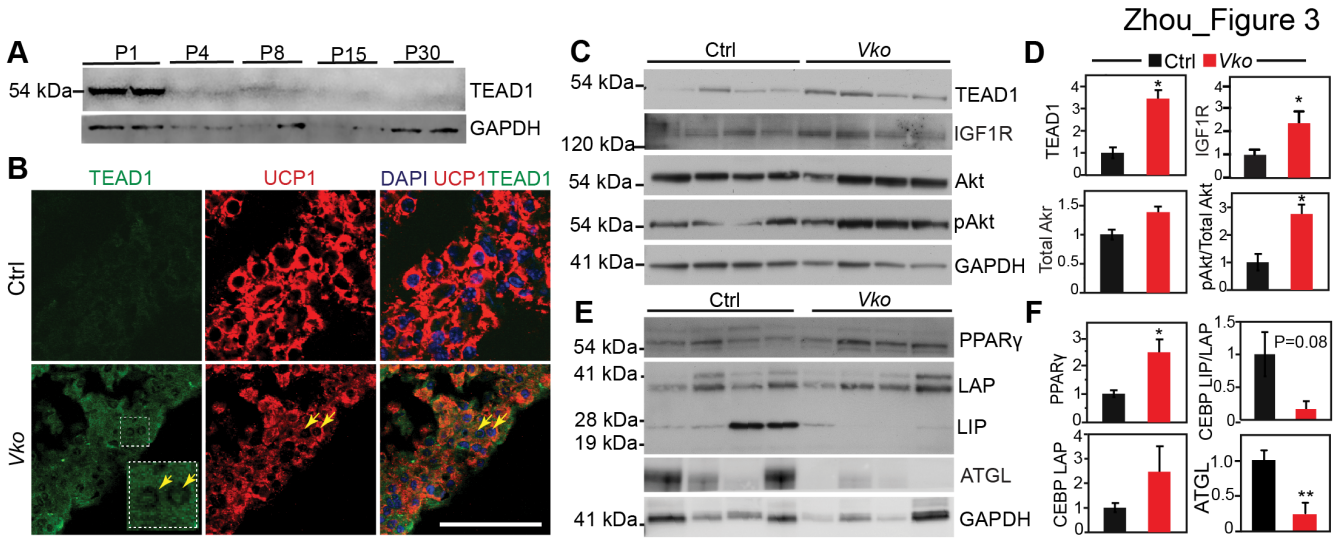

Figure 3. Loss of VGLL4 activates TEAD1. A. Western blot analysis of TEAD1 expression in BAT. BAT proteins collected from mice of different ages were compared by western blot. GAPDH was used as loading control. **B**. Immunofluorescence images of UCP1 and TEAD1 stained BAT sections. Yellow arrows indicate brown adipocytes enriched with nuclear TEAD1. Scale bar = 50 μm. **C**. Western blot analysis of TEAD1 and the crucial IGF1-Akt pathway components. **D**. Densitometry quantification of TEAD1, IGF1R, total Akt and phosphorylated Akt. **E**. Western blot analysis of crucial adipogenesis regulators. **F**. Densitometry quantification of PPARγ, C-LAP, C-LIP and ATGL. P0 interscapular BAT protein was used for western blots. D and F, protein levels were normalized to GAPDH. N=4. Student's t test, *, P<0.05; **, P<0.01.

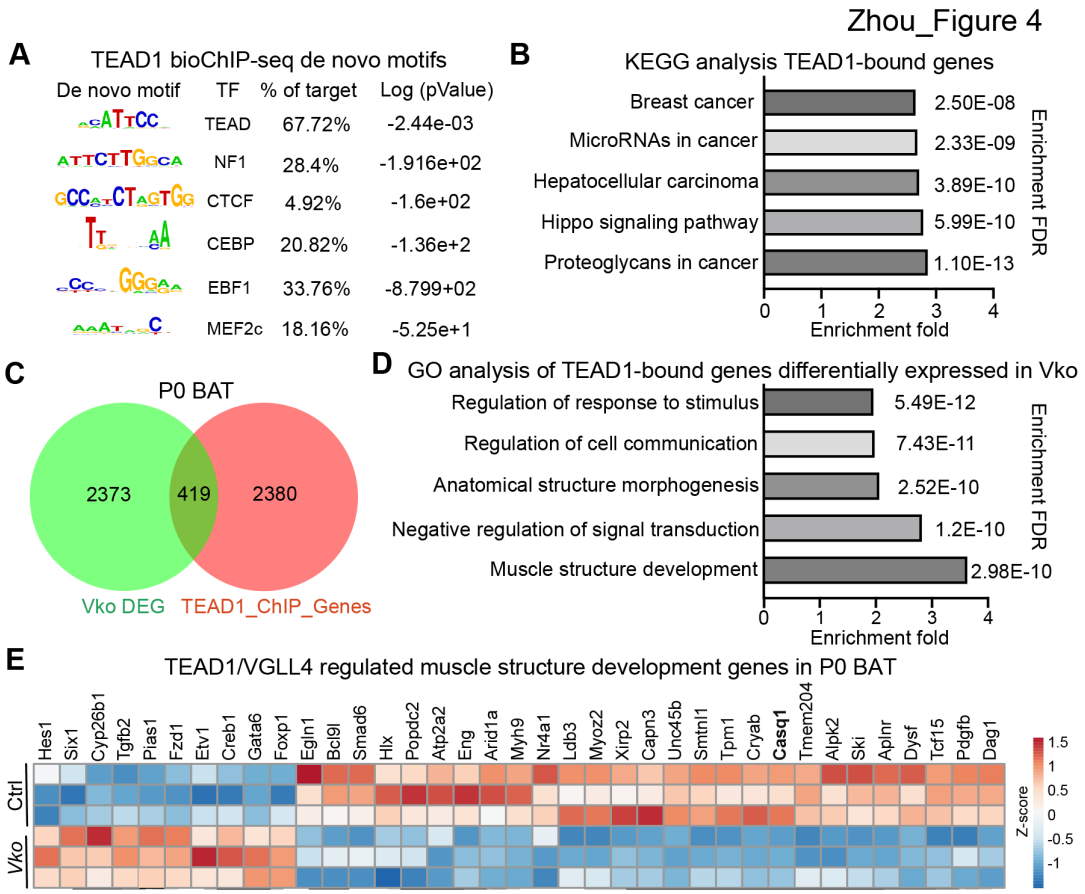

Figure 4. Identification of VGLL4/TEAD1 target genes in BAT. A. De novo motif discovery analysis within the identified TEAD1 binding sites. P0 BAT was used for TEAD1 ChIP seq. **B**. KEGG analysis of TEAD1 bound genes. The bar graph shows the top five enriched signaling pathways. **C**. Venn diagram showing the relationship between TEAD1 bound genes and differentially expressed genes in *Vko* (*Vko* DEG) brown adipose tissue. **D**. Gene Ontology analysis of the TEAD1/VGLL4 target genes. The 419 genes both dysregulated in *Vko* and bound by TEAD1 were applied to Shiny GO analysis. The top 5 enriched biological processes are listed in the bar graph. **E.** Heat map of differentially expressed VGLL4/TEAD1 regulated myogenic genes. RNA sequencing data from P0 BAT were presented. N=3.

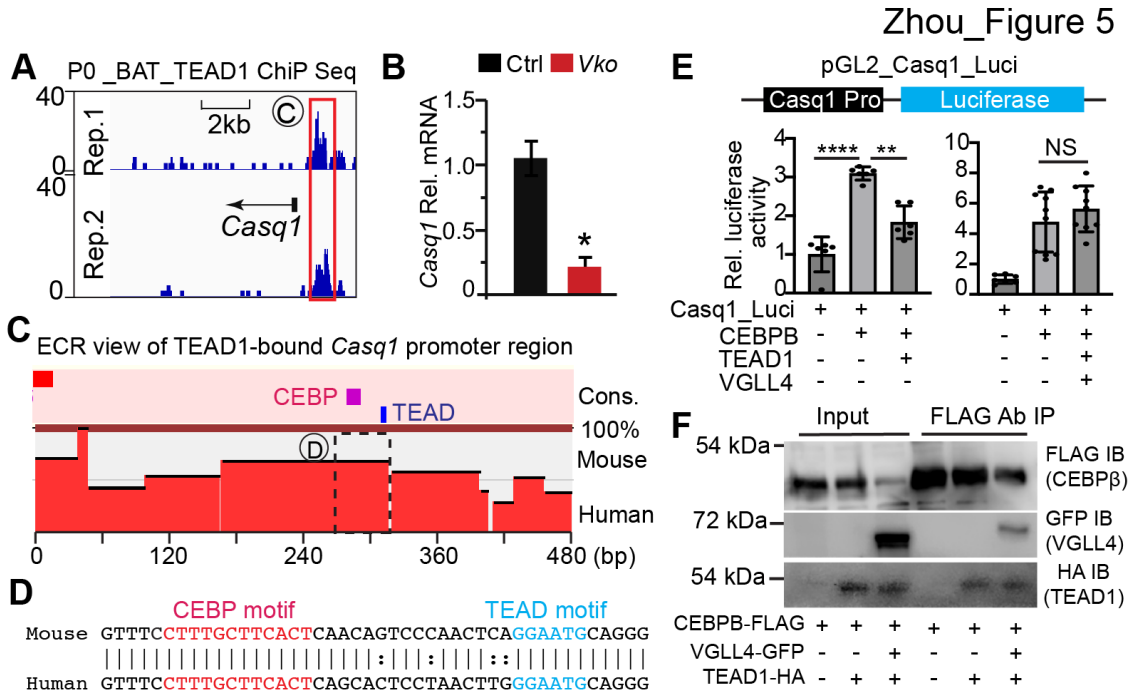

Figure 5. VGLL4 alleviates TEAD1 suppression of CEBP transcriptional activity.

A. Genome browser view showing ChIP-seq of TEAD1 occupancy near the transcriptional start site (TSS) or *Casq1*. ChIP-seq data from two biological replicates are shown. **B.** qRT-PCR measurement of *Casq1*. P0 control and *Vko* BAT mRNA was used for qRT-PCR analysis. All the tested mRNAs were normalized by endogenous 36B4 mRNA. N=4. Student t-test, *, P<0.05. **C**. Evolutionary conservation of genomes (ECR) browser view of the TEAD1-bound *Casq1* promoter region. **D**. Alignment of the mouse and human *Casq1* promoter sequences enclosed by dotted rectangle in C. Conserved CEBP and TEAD binding motifs are highlighted. **E**. Luciferase reporter assay. The TEAD1-bound *Casq1* promoter sequence was cloned into pGL2 to generate Caqs1_Luci reporter plasmid. Indicated plasmids were transfected into HEK293T cells and *Casq1* promoter activity was measured by dual-luciferase assay. N=6. One-way ANOVA followed by multiple comparison analysis, ****, p<0.0001; ***, p<0.001. **F**. Co-immunoprecipitation (Co-IP) assay. Indicated plasmids were transfected into HEK293T cells. Flag antibody was used for Co-IP.

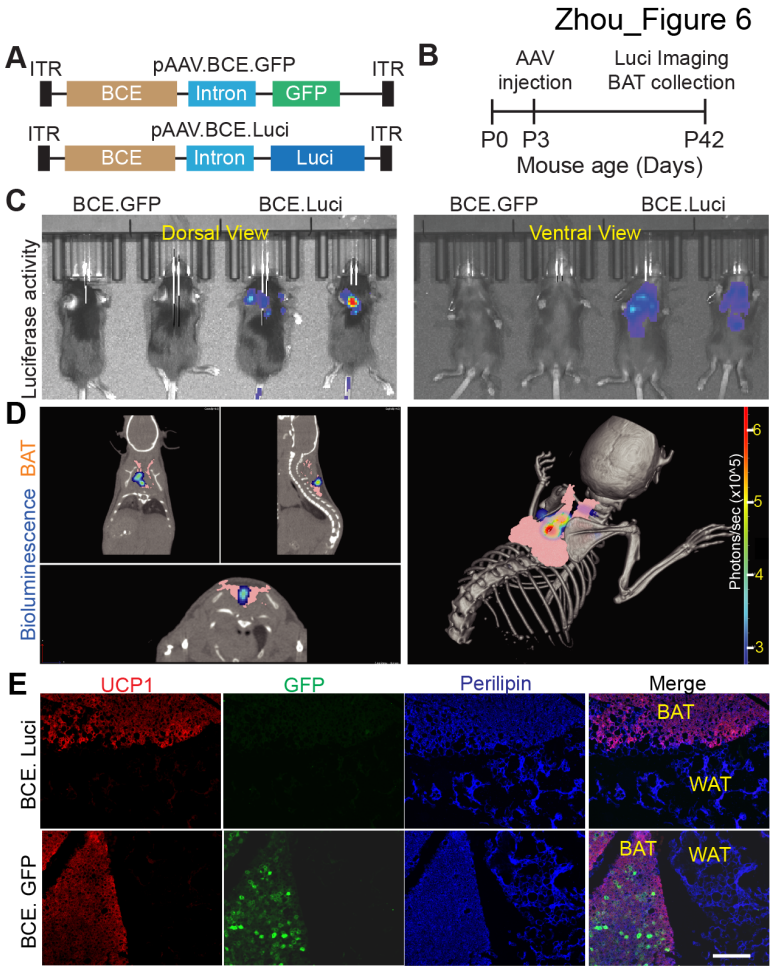

Figure 6. AAV9.BCE specifically expresses cargo genes in brown adipocytes.

A. Schematic representation of pAAV.BCE.Luci and pAAV.BCE.GFP construct. Luciferase or GFP gene was placed downstream of BCE. One chimera intron of human beta-globin and immunoglobulin heavy chain genes was placed between BCE and cargo genes to increase cargo gene expression. ITR: inverted terminal repeat sequence. **B**. Experimental design. AAV9.BCE.luci or AAV9.BCE.GFP was injected into 3 days old pups (P3) subcutaneously. At 42 days after birth (P42), bioluminescence activity was measured with PerkinElmer in vivo imaging system (IVIS). **C**. Representative bioluminescence images generated by IVIS system. Both dorsal and ventral views were presented. **D**. Representative coregistration of bioluminescence signal and *microCT* segmented interscapular brown adipose tissue from an AAV.BCE.Luci mouse highlights the origin of the biolumenscence signal within the BAT volume. Pink: brown adipose tissue. Rainbow, bioluminescence signal positive tissues. **E**. Immunofluoresence images of BAT. BAT was collected at P42 and used for immunofluorescence staining. UCP1, BAT marker protein. Perilipin: adipose tissue marker (BAT and WAT) protein. Scale bar=200 μm

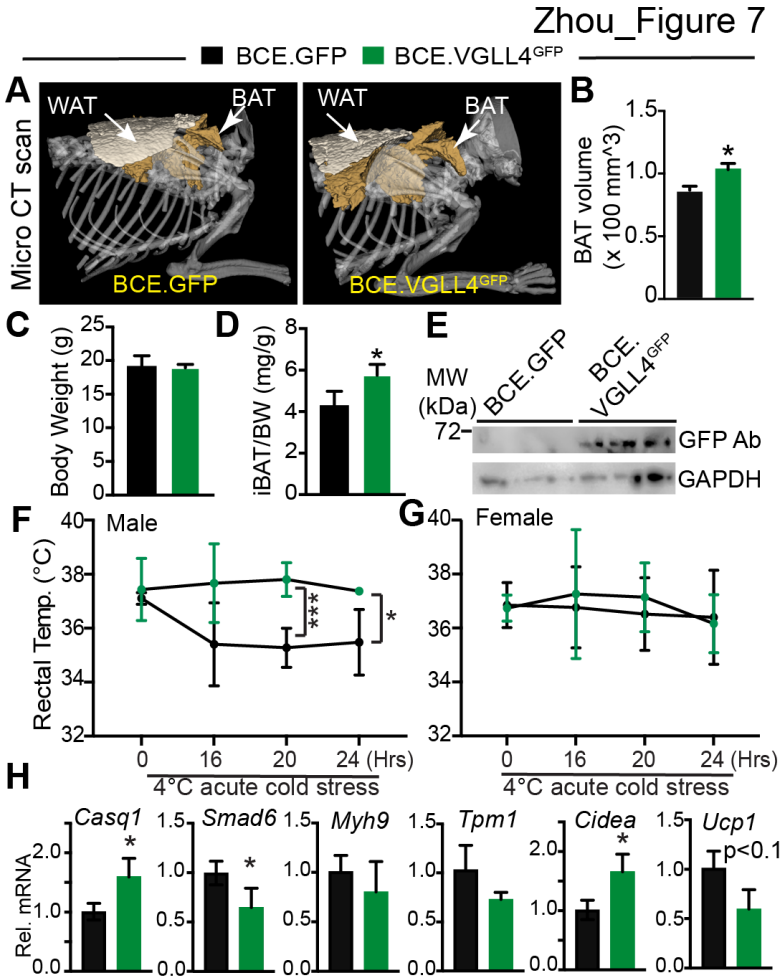

Figure 7. AAV9.BCE.VGLL4 promotes BAT growth. **A**. Representative volumetric images generated by microCT scan highlight the BAT (brown) and WAT (white) in the interscapular regions of the mice. Bones were labeled as grey. **B**. Quantification of BAT volume. **C.** Body weight. **D**. Interscapular BAT and body weight ratio. N=3. Student t-test, *, $p<0.05$. **E**. VGLL4 immunoblot with P42 BAT protein. GAPDH was used as internal control. **F-G.** Acute cold-stress test. BCE.GFP or BCE.VGLL4^{GFP} was injected into 3 days old pups (P3) subcutaneously. At 42 days after birth (P42), mice were treated with acute cold stress (4°C) for 24 hours. E, male mice rectal temperature. BCE.GFP, n=4; BCE.VGLL4^{GFP}, n=3. Student t-test, ***, $p<0.001$; *, $p<0.05$. F, female mice core temperature, n=4 for each group. **H.** qRT-PCR measurement of gene expression. P42 BAT mRNA was used for qRT-PCR analysis. All the tested mRNAs were normalized by endogenous 36B4 mRNA. N=4. Student t-test, *, $P<0.05$.